UCRL-92254, REV. 1
PREPRINT

PRODUCTION OF TRITIUM AND ^{4}He IN A LARGE CYLINDER OF ^{6}LiD IRRADIATED WITH 14-MeV NEUTRONS AND COMPARISON WITH MONTE CARLO CALCULATIONS

Eugene Goldberg, Ronald L. Barber,
Norman A. Bonner, Clyde M. Griffith,
Robert C. Haight, and David R. Nethaway

University of California
Lawrence Livermore National Laboratory
Livermore, CA 94550

This paper was prepared for submittal to
Nuclear Science and Engineering

October 1985

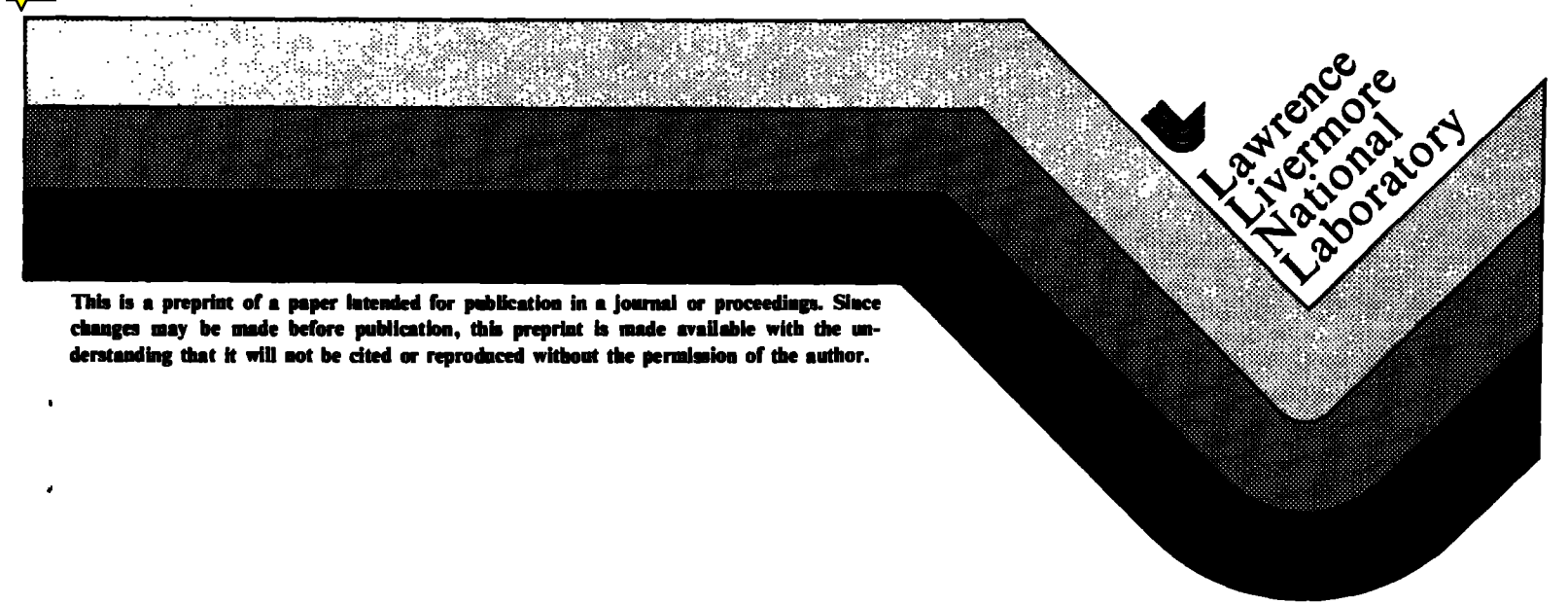

DISCLAIMER

Production of Tritium and ^{4}He in a Large Cylinder of ^{6}LiD Irradiated with 14-MeV Neutrons and Comparison with Monte Carlo Calculations

Eugene Goldberg, Ronald L. Barber, Norman A. Bonner, Clyde M. Griffith, Robert C. Haight, and David R. Nethaway

University of California
Lawrence Livermore National Laboratory
Livermore, CA 94550

Abstract

A large cylindrical assembly of ^{6}LiD was irradiated by neutrons from a high intensity D-T source. Small samples of ^{6}Li, ^{7}Li, and ^{6}LiH, all encapsulated in Pb, were positioned along the assembly axis and served as indicators for ^{4}He and tritium production. The amount of ^{4}He was determined by isotope dilution mass spectrometry while the tritium content of the ^{6}LiH wafers was measured by proportional counting of gas samples. Careful comparison of the results with TART Monte Carlo calculations showed excellent agreement. For ^{4}He generation, the experimental values were 1.01 ± 0.06 times that of the calculations, while for tritium the ratio was 1.055 ± 0.07.

Messung von Tritium und ^4He Produktion mit D-T Neutronen in einem grossen Zylinder von ^6LiD und Vergleich mit Werten berechnet mit Monte Carlo Methoden

Zusammenfassung

Eine grosse zylindrische Anordnung von ^6LiD wurde mit einer D-T Neutronenquelle von hoher Intensität bestrahlt. Proben von ^6Li, ^7Li, und ^6LiH, alle in Pb eingeschlossen, wurden entlang der Zylinderachse angebracht und dienten als Targets fuer die Produktion von ^4He und Tritium. Das ^4He wurde durch Isotopen-Dilution-Mass-Spektrometrie gemessen, während das Tritium in den ^6LiH-Scheibchen mittels Proportional-Zählern als Gas gestimmt wurde. Die Resulate waren in guter Übereinstimmung mit Werten berechnet mit TART Monto Carlo Methoden. Für die ^4He Produktion wurde das Verhältnis der experimentellen Werte zu den berechneten Werten als 1.01 ± 0.06 ermittelt, für Tritium war das Verhältnis 1.055 ± 0.07.

Production de tritium et de ^{4}He dans un large cylindre de ^{6}LiD sous l'action de neutrons provenant d'une cible de D-T, et comparaison avec des calculs bases sur la methode de Monte Carlo

Resumé

Un large cylindre de ^{6}LiD a été irradié par une source à neutron de D-T située sur son axe, près de sa face anterieure. Des echantillons de ^{6}Li, ^{7}Li et ^{6}LiH, encapsulés dans du plomb, avaient été disposés le long de l'axe et ont été utilisés pour mesurer la production de ^{4}He et de tritium. Le ^{4}He a été mesuré par spectroscopie massique de l'isotope préalablement dilué, tandis que le tritium obtenu dans les pastilles de ^{6}LiH a été detecté par comptage electronique d'echantillons gazeux. Comparaison des measures avec des calculs faits avec le code Monte Carlo TART est excellent. Le rapport des valeurs experimentales et calculées pour l'obtention de ^{4}He est de 1,01 + 0,06, pour le tritium 1,055 + 0,07.

I. Introduction

In the design of a thermonuclear energy generating facility that involves irradiation of lithium-bearing materials with D-T neutrons, one measure of performance is the amount of tritium generated. Another measure, closely related to the energy produced, is the ^{4}He generated, because the major reactions of the breeding cycle are likely to leave ^{4}He as a reaction product. Several groups have irradiated large lithium-bearing assemblies to produce tritium,[1-7] the earliest headed by M. E. Wyman who studied tritium buildup in a LiD sphere. The simple geometries generally employed, which anticipate analysis by neutron transport codes, are much more appropriate than one which reflects the complexity of an engineering design of, for example, a fusion reactor blanket.

Analysis of one of the more recent integral measurements[4] with the Lawrence Livermore National Laboratory Monte Carlo code, TART,[8] showed that the tritium actually generated exceeded by approximately 9% the TART value. Concern over this discrepancy, and a desire to attempt simultaneous measurements of ^{4}He generation, fostered the present study. Companion experiments[9] were performed in simple geometry, providing opportunities to compare inferred cross sections for 15-MeV neutrons with published, independent values.

Two irradiations, spaced three months apart, were performed with a large cylindrical ^{6}LiD assembly. The geometry was essentially two-dimensional, to simplify analysis. Considerable attention was given to the neutron source, the RTNS-I facility of Lawrence Livermore National Laboratory,[10,11] both experimentally and in the code model.[9] The neutron fluence was primarily determined with nuclear activation foils of niobium, gold, zirconium, yttrium and indirectly, aluminum, the latter through the reaction,

$^{27}Al(n,\alpha)^{24}Na$. Special small capsules of metallic ^{6}Li or ^{7}Li encased in lead, and wafers of ^{6}LiH or ^{7}LiH also encased in lead were accurately positioned along the axis of the large assembly. The capsules were designed for mass spectrometric analysis of ^{4}He while the larger wafers were analyzed for tritium content.

II. Experimental Procedure

II. A. Neutron Source Characteristics

An intense neutron source was chosen to give large fluences of neutrons and thereby to enhance the signal-to-background ratios for the measured quantities. The RTNS-I neutron source has been described in detail earlier[10,11] and in a companion paper.[9] Briefly, it consists of a 10-20 mA beam of 400 keV D^{+} ions incident on an internally cooled copper-alloy disk rotating at 1100 rpm which is internally cooled with water. The disk is 1.5 mm thick and the surface struck by the beam is coated with titanium which in turn is loaded with tritium. The rotating target is adjustable relative to the beam in a transverse direction, permitting movement to a fresh band of titanium tritide as the neutron yield drops. The beam spot diameter is nominally 10 mm. Under typical operating conditions, a yield of about 2×10^{12} n/s is realized.

Prior to the integral measurements, the intensity of the neutron field was studied using aluminum foils positioned at various angles with respect to the beam. The ^{24}Na activity revealed an appreciable dip in the field of about 30% at 90 deg due to scattering of the source neutrons by the rotating target. Reference 9 deals with this topic in detail.

The energy spectrum of the source neutrons was examined by measurements

of (a) the neutron yield vs deuteron energy, (b) the ratio of induced activity of selected isotopes and in particular $^{90}Zr(n,2n)^{89}Zr$: $^{27}Al(n,\alpha)^{24}Na$, and (c) the pulse height distribution of $^{29}Si(n,\alpha)^{25}Mg$ events registered in a silicon surface barrier detector. Reference 9 also assesses these techniques. The results for the two irradiations are discussed invididually below.

II. B. Cylindrical ^{6}LiD Assembly

For the sake of brevity, the configuration for only the first irradiation will be discussed in detail. The two irradiations had a great deal in common.

Figure 1 illustrates the physical arrangement of components. The ^{6}LiD cylinder, whose nominal diameter and thickness are 900 mm and 500 mm respectively, was in two parts. A cylindrical shroud of ^{6}LiD, 150 mm thick, encircled the source and prevented unnecessary loss of neutrons.

II. B.1. ^{6}LiD Components

The parameters of the ^{6}LiD itself are given in Table I. These three parts were each enclosed in welded stainless steel to prevent attack by water vapor and in addition were coated with a plastic. The outer cylindrical surfaces were covered with 0.81-mm stainless steel sheet, the plane surfaces with 0.51-mm sheeting, and the inner surface with a stainless steel tube of 0.25 mm wall thickness.

Core samples were removed during the drilling of the sample holes in the blocks and densities were measured to be 0.775 and 0.778 Mg/m^3. An average for the blocks was then

$$\rho\ (^{6}LiD) = 0.776 \pm .002\ Mg/m^3$$

with the uncertainty accounting for the spread in measurements. Chemical and isotopic analyses showed the ^{6}LiD assembly to consist of:

$$^{6}Li_{.9564}\ ^{7}Li_{.0444}\ H_{.0088}\ D_{.9888}\ O_{.0016}$$

with a multitude of minor impurities combined in the oxygen fraction.

A foil holder, enlarged in Fig. 1, was interposed between the rotating target and sample hole, along the beam axis, to provide a means of accurately determinating the location and size of the neutron source. It was nominally 5 cm in length, and the measurements of the activation levels of the foils in comparison to TART calculations provided the axial position of the source to within an uncertainty of 0.5 mm as determined from earlier experiments.

The sample hole, also shown in Fig. 1, was designed to contain 24 samples for ^{4}He measurements, 12 samples for tritium measurements, and otherwise be filled with ^{6}LiD spacers. Gold, yttrium, zirconium, and niobium foils were located along the sample hole to provide measurements of the shielding character of the assembly, but more importantly they enabled us to determine the neutron source strength to an accuracy of ∿3-4%. The hole of each block was lined with a stainless steel tube of 0.25 mm thickness, as mentioned above, and 26.04 mm I.D. The components of the sample string were assembled in a mylar tube of ∿ 0.10 mm thickness and slipped into the hole as a unit.

II.B.2. Contents of Sample Hole

A modular scheme was employed in assembling the sample string. The basic module contained four foils, of gold, zirconium, yttrium, and niobium, followed by a cylindrical wafer of ^{6}LiD with a depression designed to accommodate two Li/Pb capsules for ^{4}He measurement. This "cup" was followed

by a cylindrical wafer of ^{6}LiH, encased in lead, for tritium measurements. The module was nominally 10 mm thick. At greater depths, these modules were separated by ^{6}LiD spacers, each of 10 mm nominal thickness. The ^{6}LiD components were thinly coated with plastic to protect them from attack by water vapor when exposed to air.

II.B.2.a. $^{6}Li/Pb$ Capsule (^{4}He Measurement)

The design, development, and fabrication of capsules containing lithium for ^{4}He measurement required care so that no ^{4}He escaped and so that interfering reactions were kept to a minimum. We settled on a thin lead-walled capsule with dimensions appropriate to the sample hole and with a mass and shape compatible with the furnace manifold attached to the mass spectrometer at Rockwell International Energy Systems Group (R-I), Canoga Park, California where the ^{4}He analysis was carried out. Initially the active material was to be ^{6}LiD. This we abandoned after a short time upon realization that D_2 would overwhelm the minute ^{4}He spectrometer signal. We eschewed ^{6}LiH also, anticipating that HD would be confused with the ^{3}He spike. In addition, the hydrogen would have to be gettered, and our samples were anticipated to exceed the gettering capacity of the R-I facility, thus requiring expansion of the gettering capacity and frequent changes.

The design chosen for the capsule was nominally 60 mg of lithium (95.6 atom % ^{6}Li) contained in lead for a total mass of 860 mg. The O.D. was 3.81 mm, and nominal length was 17.8 mm. The lead wall was 0.25 mm thick while the caps were 0.51 mm thick. No voids were allowed in the capsule. The cylindrical slug of lithium metal was sealed under vacuum to avoid inclusion of trace amounts of He expected to be in the drybox atmosphere.

Lead was chosen for a number of reasons. First, the ^{4}He-production

cross-section at $E_n \sim$ 15 MeV as measured by Kneff[12] of R-I is very small - 0.62 mb - and so would not contribute a measurable fraction of ^{4}He upon vaporization. Secondly, lead should insure containment of the ^{4}He produced: ^{4}He is very insoluble in Pb at room temperatures. Further, the lead is easily melted and vaporized in the R-I furnace. Also, because lead is so soft, fabrication of the capsule and sealing were expected, and were found to be, relatively trouble-free.

After some unsuccessful attempts to speed development, we developed the following procedure, which was found to produce a product whose baseline (i.e. unexposed to neutrons) ^{4}He content, as determined by R-I measurements and prototypes, was $\sim 2 \times 10^{10}$ atoms of ^{4}He. The lead (99.99% pure) was first melted and maintained for at least 18 hrs at 520°C under vacuum to drive off any ^{4}He. The material was then cooled and rolled to a thickness of 2.0 mm, and circular disks about 10 mm in diameter were punched out and placed in an extrusion press which produced a tube of 0.25 mm wall thickness sealed at one end. The excess lead was left as a flared cone and, before removal, the tube was vacuum tested for pinholes and flaws using the flared portion as a gasket. The tube was cut to length and also its closed end was shaped to match the shape of the ^{6}Li slug which was to be inserted. Caps of lead 0.51 mm thick were fabricated from the vacuum-melted stock. The tube and cap were weighed.

The ^{6}Li metal was also melted under vacuum and held at a temperature of 670°C for 24 hours. After cooling, a strand 3.18mm in diameter was extruded. This was then sheared in a special cutting assembly to a length of 16.8 mm, and weighed.

The ^{6}Li slug was inserted into the vertical tube and gently settled to the tube bottom. The cap was placed in the tube over the ^{6}Li, the tube lip

was then bent gently inward with a simple tool to clamp the lid in place and finally the unit was placed in a press. The tube was evacuated prior to sealing, and then 172 MPa gage (25000 psi) was briefly applied while the tube was under vacuum. The excess lead flowed locally to seal the capsule. Upon removal the capsule was weighed to verify that all material was accounted for, after which any Pb which was loosely connected to the capsule was trimmed away.

After fabrication, the capsule was immersed in anhydrous ethyl alcohol. If any lithium was exposed, bubbles would emanate from the lithium sites. Only those capsules which were free of bubbles were accepted. The procedure tended to limit possible leak sites to the cap area, and so further inspection was made with a stage microscope, concentrating on the capped end of each capsule.

II.B.2.b. ^{6}LiH/Pb Wafer (Tritium Measurement)

For tritium measurement, ^{6}LiH wafers were encapsulated by lead foils 0.25 mm thick to produce samples 3.5 mm thick and 25.4 mm in diameter. The details of fabrication and the wafer performance are discussed in Ref. 9. For both ^{6}LiH and ^{7}LiH wafers, the nominal hydride mass was 1.0 g.

Possible tritium loss was less of an issue for these wafers than for ^{4}He loss from the Li/Pb capsules because the hydrogen of the ^{6}LiH acted as a carrier for the tritium, and loss of a significant portion of tritium would have been signaled by a corresponding loss of hydrogen. The measurement was in units of atoms of tritium per atom of hydrogen which is quite satisfactory for our purpose. The lead coating served more as a seal against attack by water vapor than as a tritium barrier.

II.B.2.c. Placement of Sample Tube Components

Table II lists the components of the sample tube for the first irradiation. The cups, wafers, and spacers were of very uniform quality, with the masses for individual samples of a given type within one percent of the mean, while ^{7}Li masses varied even less. The average characteristics (used to develop the modular parameters for TART) are:

Foils; thickness (mm):

Au:	#1-17	(.051)
Nb:	#2-5	(.079)
Nb:	#1,6-17	(.137)
Zr:	#5	(.127)
Zr:	#6-17	(.114)
Ni:	#2-5	(.025)
Y:	#6-17	(.145)

Capsules:

^{6}Li, isotopic purity 95.5%
Li mass: .06054 g
Pb mass: .9171 g

^{7}Li, isotopic purity 99.99%
Li mass: .0699 g
Pb mass: .8852 g

Pb:
Tube: Pb mass: .840 g
Sheet: Pb mass: .185 g
Wire: Pb mass: .184 g

^{6}LiD cups, isotopic purity: 95.6% ^{6}Li

Mass: 1.752 g
Thickness: 6.303 mm
Depth of trough: 4.043 mm

Wafers, isotopic purity: 95.6% ^{6}Li

Mass: .9678 g ^{6}LiH (95.6% ^{6}Li)
3.8378 g Pb
Thickness: 3.503 mm

^{6}LiD spacers, isotopic purity: 95.6% ^{6}Li

Mass: 3.9461 g
Thickness: 10.00 mm

The axial spacing between the frontal face of the leading gold foil and frontal face of the ^{6}LiD of the large assembly (where the sample hole begins) was 45.4 mm. The stainless steel sheet pressed against the face was 0.51 mm thick.

All components slipped into a mylar tube of 25.4 mm I.D. and 0.10 mm thickness. The cups' diameters were slightly undersize while the wafers and spacers fit snugly in the tube. The disparity was taken into account in the calculations.

The capsule pairs were wrapped in .025-mm-thick lead sheets to insure that any ^{4}He produced in adjacent materials could not become imbedded from the outside in the capsule walls. Segments of lead wire were placed alongside the capsules to provide additional means to assess ^{4}He production in lead, but we chose not to analyze them because with the empty lead capsules adequately served that purpose.

The procedure for positioning the ^{6}LiD assembly began by determining the source position by irradiating a copper foil and subsequent autoradiography. The assembly, with the sample tube removed, was then aligned with its axis along the deuteron beam axis. The ^{6}LiD cylinder face was located nominally 5 cm from the target outer surface and the distance was measured for later specification in the Monte Carlo calculations. Finally the sample tube was inserted with a 1.0-mm shim between the target outer surface and upstream face of the sample tube. The shim was removed prior to the irradiation. This 1.0-mm spacing was expected to give only an approximate representation of the actual gap during the irradiation because of (a) deformation of the target during rotation, (b) inaccuracies of the measurement due to poor visibility (we used a mirror), or (c) variations in the spacings for different bands on the target. We believe these uncertainties amount to

to no more than 0.5 mm total uncertainty in the spacing. We depended upon interpretation of the activation foils for a more accurate determination of location of the sample tube contents with respect to the source spot.

III. TART Calculation for Irradiation 1

Figure 2 illustrates the geometry of a key TART problem which modelled the first irradiation. Sixty-seven minutes of Cray-I time were consumed for 4 x 10^6 source neutrons in the calculation which involved 150 spatial zones. We did not employ particle weighting for the study of the first irradiation. The statistical uncertainty of the Monte Carlo calculations of ^{4}He and tritium production was kept within the accuracy of the measurements. The same model for the source (i.e. multi-angle, multi-energy) used in Ref. 9 was used here.

To reduce the statistical noise of the TART calculations of ^{4}He and tritium generated within the respective small zones, parallel problems considerably simplified and with large zones were run to get the shape of the tritium- and ^{4}He-generation curves. These were used to guide us in fitting smooth curves through the points generated in the detailed TART calculations. The ratios presented here of experimental to calculated ^{4}He and tritium production referred the experimental values to these smoothed curves. We believe the comparison to be improved by such a procedure.

To avoid the tedium of specifying each component explicitly in the TART calculations, modular descriptions were constructed with care so that axial positions were altered by no more than ± 0.15%. Masses in the Monte Carlo model were generally within 1% of the actual values.

IV. Experimental Results for Irradiation 1

IV.A.Neutron Source Characteristics

IV.A.1. Source Spectrum and Size

On the day prior to start of the prolonged irradiation, we sought to characterize the source by a few of the techniques discussed above. First we shifted to a relatively fresh band on the rotating disk, and with the ^{6}LiD assembly far removed from the target area generated a Neutron Yield vs E (Deuteron) curve. We found, in contrast to the yield vs. deuteron energy correlation of Ref. 9, a neutron yield which agreed within 10% with the fresh target yield of Seagrave (assuming TiT)[13] and also with our newly generated curve (assuming $TiT_{1.5}$).[9,14] This result suggests a uniform tritium loading and therefore, a value for the average neutron energy ($\bar{E}_n$) of 14.98 MeV in the forward direction with respect to the incident deuteron beam direction.

For further calibration of the neutron energy we observed the pulse height distribution (p.h.d.) of neutron-induced events in a silicon surface barrier detector. First we positioned the detector at at θ = 96°, to calibrate the energy scale and to determine the detector resolution. We then moved the detector to 180° and used the $^{29}Si(n,\alpha_0)$ peak as an indicator of the average energy of the source neutrons as in Ref. 9. The average neutron energy was found to be constant within 50 keV over the course of the irradiation.

After the 47 hour irradiation was completed, autoradiographs of the gold and niobium foils closest to the neutron source were made to show the shape, size, and transverse location of the source. We found the spot to be $\sim$ 10 mm in diameter and centered to within 1 mm, with respect to the activation

foils at the face of the sample tube. Consequently, in the TART calculations, the source disk was assigned a 5-mm radius and was centered on the cylinder axis.

IV.A.2. Source Strength

The neutron source intensity averaged approximately 1.8×10^{12} n/sec over the length of the irradiation. An accurate value for the strength was inferred from the four families of activation foils accurately located within the sample tube. These are of gold, niobium, zirconium, and yttrium. The few nickel foils in the forward region were not utilized because of lack of confidence in their cross sections. Since the ^{6}LiD assembly influences the activation values significantly, especially at greater depths of penetration into the ^{6}LiD, this process of inferring source strength involves careful reference to the TART calculations.

Two proton recoil counters, which viewed the neutron source at production angles of 135 deg and 145 deg and at distances of 1.00 m, were also employed. These were meant to act as absolutely calibrated flux monitors for the bare source. However, in this situation, the massive ^{6}LiD assembly reflected neutrons back to these counters. An experiment showed the enhancement factor to be 1.11. A TART calculation gave a factor of 1.17. This discrepancy could be due to the counter bias setting procedure. Where the counter data was used in the following analysis, the experimental enhancement factor was assumed.

Figure 3 illustrates the Z^2 x (product atoms/g of activation foil) for the four sets of foils employed, with (Z) measured from the source plane. We selected a gap of 0.65 mm between the rotating target outer surface and frontal surface of the leading gold foil for reasons to be discussed below. The statistical accuracy of the counts per foil was generally ± 1%. Each

set follows a smooth curve. The gold and niobium sets were less attenuated than the zirconium and yttrium sets since the latter have distinctly higher reaction thresholds [all (n,2n)] than the former. TART calculations were run to determine the source strength accurately. The TART-generated function:

$$\psi = Z^2 \times (\text{atoms of radioactive product/g of foil})/\text{source neutron}$$

was found to be rather insensitive to the choice of gap size between target and leading gold foil. Since we display in Fig. 3 the directly measured (Z^2 x atoms/g), the corresponding quantity is (ψ x S) so the source strength is simply a multiplier. The excellent quality of the data encouraged us to seek a match to greater depths of ^{6}LiD - and indeed we see in general very good agreement between slopes for all four sets out to values of Z = 200 mm. By using a gap of 0.65 mm in the code (which, when added to the 1.52-mm thickness of the backing of the rotating target, is equivalent to an axial spacing of 2.17 mm between the source plane and front face of the leading gold foil) we were able to achieve fairly good fits for the measurements with Z>5 cm in the cases of niobium and gold.

The gold and niobium foils closest to the source were first counted, and then small 3.2-mm-diameter disks were punched from each foil central region and counted. By discounting the closest data point (which is extremely sensitive to the source-disk spacing) and insisting on good fits for the other data points, we find for the niobium foils (Z < 200 mm) a source strength of 2.98×10^{17}n with a standard deviation of 1% of the mean. The ^{93}Nb(n,2n)^{92m}Nb cross sections used by TART were a special set drawn from a compilation supplied by Nethaway.[15] A small increase of 0.5% was incorporated to account for the difference between the reference

$^{27}Al(n,\alpha)^{24}Na$ cross sections used by Nethaway (who measured the niobium cross section relative to the aluminum value) and the more recent evaluation of Tagesen and Vonach.[16]

From the $^{197}Au(n,2n)^{196}Au$ data we infer a source strength of 2.94 ± 0.10 x 10^{17}n using the findings of Ref. 15 corrected by 0.5% as we did above. We used here the TART cross section set corrected by a multiplier based on an average over the Seagrave spectrum of 2.11 b for the TART set and 2.16 b for the set recommended by Nethaway.[15] The fit as a function of depth was not as good as in the case of niobium, suggesting the possibility that the cross section for gold is not accurately portrayed away from the high energy peak.

The $^{90}Zr(n,2n)^{89}Zr$ cross section has also been carefully measured with respect to the $^{27}Al(n,\alpha)^{24}Na$ reaction.[17] The cross sections used as input to TART produced values which were then adjusted by 0.4% to account for the modest difference with Pavlik's[17] findings. The isotope fraction for ^{90}Zr is taken at 0.515. A source strength of 3.03 ± .05 x 10^{17}n was found.

The yttrium set by similar calculations led to a source strength of 2.94 x 10^{17} ± 0.04 n. In spite of the fact that fewer foils were exposed, this value is in excellent agreement with the source strength determined from the other activation foils.

We are also able to estimate the source strength from the proton recoil counter data. Using the reflection correction of 1.11 arrived at experimentally, we find a source strength of 3.06 x 10^{17}n. A grand average, with all five values equally weighted, is 2.99 x 10^{17}n.

We choose finally a source value:

$$S = (2.99 \pm .09) \times 10^{17} n$$

with the uncertainty reflecting statistical and estimated systematic uncertainties.

IV.B. Tritium in ^{6}LiH

Eleven of the twelve ^{6}LiH wafers in the sample tube provided acceptable data. The ^{6}LiH wafers (95.5% ^{6}Li) employed in the overall study came from a common stock so many background samples could be intercompared. The tritium results were specified in units of [atoms tritium/liter H_2(STP)], since the wafer material is decomposed in the analytic process. The measurement accuracy has been specified at 2%, after intercalibration with an NBS standard sample.[9] The average background value, from five samples, was $4.9 \pm 1.5 \times 10^{10}$ atoms tritium/liter H_2(STP). On the average, each wafer released 1.53 liters H_2(STP) upon decomposition.

Table III lists the experimental values of tritium released for each capsule. We see the background to be a very small fraction of the measured values - even for the deepest wafer, the background is only $\sim$ 8% of the gross measurement. The uncertainty in the background, only $\sim$ 2.4% of that foreground, is more relevant to the error analysis. Figure 4 illustrates the findings.

IV.C. ^{4}He in ^{6}Li and ^{7}Li

Table IV summarizes the ^{4}He findings of the first RTNS-I run. The capsules at the deepest positions (Z > 23 cm) were not analyzed because the

background capsules from that batch registered excessively high ^{4}He levels. The batch which included all the others was limited in number. Their background, taken at 7.6×10^9 atoms per capsule, was based on one reading plus the trend at that time among the capsules tested during development. Figure 5 illustrates the experimental results for the ^{6}Li capsules. The deterioration of quality at greater depths is evident.

An accuracy of 2% is attached to the mass spectrometeric analysis of the ^{4}He by the R-I group, based on detailed attention to the calibration of the detector and many years of experience.[12,18] The smooth behavior of the experimental points in Fig. 5 suggests that additional contributions to the spread about the correct values are generally modest.

V. Experimental Results for Irradiation 2

The second irradiation run, planned from the outset, served well to demonstrate the reproducibility of the data. Quality control, particularly regarding the lithium capsules used for ^{4}He measurements, was a potential problem, and intercomparison of data from the two runs helped greatly to expose spurious readings.

The second irradiation was the more ambitious of the two. In addition to a set of samples similar to the original set, we placed ^{7}LiH wafers in the sample hole and ^{6}Li capsules and ^{6}LiH wafers at greater depths. Five ^{7}Li capsules were exposed. Activation foils were emplaced more deeply as well. The second irradiation was of 66 hour duration, and the target was fresh at the outset. The silicon surface barrier detector demonstrated that the average neutron energy varied by less than 50 keV of its starting value, expected to be $\bar{E}_n$ = 14.98 MeV.

The best fit of TART-generated foil activation values to the experimental

results was achieved with a gap of 1.40 mm between the outer surface of the source disk and frontal face of the leading gold foil (implying an axial spacing between source plane and Au frontal face of 2.92 mm). Prior to the irradiation, the gap was measured to be 1.1 mm. For this irradiation, the axial distance between the frontal faces of the leading Au foil and ^{6}LiD of the assembly was 41.4 mm, which was 4.0 mm shorter than in the first campaign. The fluence determined by the recoil counters was assigned a 5% uncertainty. The calibration was modified by the count enhancement factor of 1.11 described above. Utilizing the data from the gold, niobium, zirconium, and yttrium foils as well as the proton recoil counters, the source strength was found to be

$$S = 4.99 \pm 0.20 \times 10^{17} \text{ n}$$

with $\bar{E}_n$ = 14.98 MeV and a spectrum as given by Seagrave (see Ref. 9 for a discussion of the applicability of this spectrum).

Figure 6 illustrates the activation foil data for the second irradiation, assuming a 1.4 mm gap. The data are presented as $(\Delta Z)^2$ x (Activity) to highlight the attenuation of the ^{6}LiD. The quality of the data is quite good revealing exponential dropoffs of activity at greater depths.

The ^{4}He and tritium measurements will not be listed explicitly here for brevity. However the findings will be included when comparison is made to TART calculations. We note that the ^{4}He backgrounds per capsule for the batches used in the second irradiation were for ^{6}Li : $9.2 \pm 4.6 \times 10^{10}$ atoms and for ^{7}Li: $8 \pm 8 \times 10^{10}$ atoms. At the station closest to the source the ^{6}Li capsule registered 550×10^{10} atoms ^{4}He while the ^{7}Li capsule registered 262×10^{10} atoms ^{4}He.

The tritium background correction for the ^{6}LiH was more modest: $4.9 \pm 1.5 \times 10^{10}$ atoms T/liter H_2(STP). The shallowest wafer registered 1418 x

10^{10} atoms T/liter H_2. A few outlying points suggesting contamination levels of 4×10^{12} atoms T/liter will be apparent in a later illustration.

The tritium background for the ^{7}LiH wafers was found to be excessively high. Isotopic analysis showed the ^{7}LiH to contain deuterium in variable quantities, that is $^7Li^2H$. The deuterium is generally accompanied by tritium in the isotopic enrichment process as in this case. We therefore could not derive values for the tritium production values for ^{7}Li from this experiment.

VI. Comparison to TART Monte Carlo Calculations

The TART code calculates, per source neutron, the tritium or ^{4}He per zone assigned to the actual wafer or capsule. A quantity which provides a convenient intercomparison of the two irradiations is the ratio of the product generated in the experiment to that in the calculation as a function of distance of detector from the source. For example, the ^{6}Li capsule ratio for ^{4}He generation is:

$$R_\alpha = \frac{(\text{atoms } ^4\text{He per capsule})_{exp}}{S(\text{atoms per capsule per neutron})_{TART}}$$

where the denominator contains the source strength inferred experimentally and the TART value for ^{4}He is taken from the smoothed curve through the calculated points discussed earlier.

VI.A. Tritium in ^{6}LiH Wafers

Analysis of the tritium produced in ^{6}LiH wafers near the neutron source requires special attention since the neutron spectrum there is relatively undegraded, and such neutrons are relatively ineffective as tritium generators. The companion study[9] in which ^{6}LiH wafers were

directly exposed to 15-MeV neutrons led us to examine in detail the effects of various perturbations that were not initially included in the TART calculations. These included D-D neutrons from deuterium buildup in the target and beam collimator scattering. The influence of both of these effects quickly subsided as deeper wafers were considered. TART calculations were performed to study the effects of the more important issues. We found, for example, that tritium production was enhanced by 9 ± 4% for the ^{6}LiH wafer closest to the source when all these effects were included. The D-D correction, 4% for this sample, was the largest, and the collimator correction (2%) was next. At the next station, the enhancement dropped to 6 ± 3%.

One mechanism which could have introduced tritium into the wafer in this experiment but not in that of Ref. 9 was the recoil of tritons created in adjacent ^{6}LiD capsule cups and spacers. These items were painted with a thin (.025 mm) plastic coat to prevent attack by water vapor. Since the tritons arising from the $^{6}Li(n,T)\alpha$ reaction generally have a range in ^{6}LiD or CH_2 of about 6 mg/cm^2, a calculation shows that the wafer tritium content would be enhanced by 0.5% at most. We therefore discount this correction.

Figure 7 summarizes the tritium production results for the two integral measurements in terms of the ratio of experimental to calculated values. Three points outside the range of the other data occurred in the second irratiation. The data from the first irradiation did not exhibit any anomalies out to a distance of 340 mm, or about 300 mm into the ^{6}LiD. None of the ratios is below a value of 1.01, and if the three deviant points are discounted, the average ratio, weighted according to the local specific tritium production, is

$$\left(\overline{\text{Exp./Calc.}}\right)_{\text{Tritium in } {}^{6}LiH} = 1.055 \pm 0.07 \quad .$$

The uncertainty (1 standard deviation) was obtained by summation in quadrature of the uncertainties from the components participating in the determination of the ratios. The major contributor to the uncertainty, except at large depths, was the source strength uncertainty, which was estimated as ± 3% for the first run and ± 4% for the second. Beyond a distance of 300 mm, Monte Carlo statistics was the major contributor to the uncertainty for the first irradiation. The ratio is seen to be within one standard deviation of unity.

VI.B.1. ^{4}He in Li/Pb Capsules

Figure 8 summarizes the findings for the production of ^{4}He in the ^{6}Li capsules for the two irradiations. Recall that the data show a peak in the product $Z^2 \times {}^{4}He$ content per capsule at $Z \sim 180$ mm (Fig. 5). At closer distances we see the ratio of experimental to calculated values to be generally within 5% of unity. At larger distances, some apparently discrepant points are evident.

The group of points at $\Delta Z \sim 210$ mm shows a clear disparity between the two irradiations - the points from the second are near unity while those from the first are more than two standard deviations away. The error bars represent the cumulative uncertainty in ^{4}He measurements, and Monte Carlo statistics. In this case, the points from the second irradiation should be given more weight, because we have a much more detailed understanding of the ^{4}He content of the background capsules for that case than we have for samples used in the earlier irradiation.

Our capsules were fabricated following a procedure which sought to reduce the background ^{4}He content to less than 5×10^{10} atoms per capsule. We employed a vacuum melt procedure, monitoring the ^{4}He as it was released. Apparently this procedure does not provide a uniform product. One possible

explanation may be gleaned from recent materials studies motivated by questions relevant to controlled fusion reactor design. Evidence has accrued[19] that indicates clustering of helium atoms in the host medium thereby hindering the escape of the helium. Our procedure in which the ^{6}Li was heated under vacuum at 670°C for 24 hr apparently was not adequate to generate a uniform helium-free product. Judging from the variation among background samples, we surmise that the residual helium after the vacuum melt is markedly nonuniform throughout the lithium.

Monte Carlo calculations show that at a distance of 200 mm from the source, the tritium generated in ^{6}Li is about 60% of the ^{4}He generation, and the ratio rises to 72% at greater depths. If, then, the high results for tritium production signal a real peak, the ^{4}He data should manifest a peak at the same physical position, and vice versa. Coincidence does not appear to occur, strengthening our inclination to discount the unexpectedly high points. When this is done, a straightforward average of the ratio of the experimental to calculated ^{4}He content, weighed by the axial profile (i.e. Fig. 8), results in

$$\overline{(Exp./Calc.)}_{^{4}He \text{ in } ^{6}Li} = 1.01 \pm 0.06 \quad .$$

We may then conclude that the current TART Monte Carlo model with its present set of neutron cross-sections is in close agreement with the integral experiments discussed here, insofar as ^{4}He generation in ^{6}Li is concerned.

VI.B.2. ^{4}He in ^{7}Li/Pb Capsules

Four ^{7}Li capsules were successfully exposed in the first integral measurement and five in the second. Background capsules were respectively one

and two in number. No buildup, as in the case of ^{6}Li, was anticipated, so the capsules were positioned relatively close to the source. For the farthest capsule in the second irradiation, ΔZ (source-capsule center distance) was 183 mm, and the uncertainty in background was 32% of the total measured ^{4}He.

The quality of the data at very shallow positions, where the signal is primarily due to neutrons undegraded in energy, appears to be satisfactory. We may extract a cross section value at E_n = 15 MeV, by assuming the relative dependence of cross section on energy is correct in the TART calculation. For the forward capsule station, TART calculations show a $\sim$ 6% enhancement in ^{4}He production in ^{7}Li due to the ^{6}LiD assembly. If we weight the cross-section values by (total ^{4}He content)^{2}, we find:

First irradiation: $\sigma_7(n,x\alpha) \simeq 301$ mb (E_n = 15 MeV)

Second irradiation: $\simeq 317$ mb (E_n = 15 MeV)

8-4-83 (free-in-air): $\simeq 336$ mb (E_n = 15 MeV)

The last entry, to be discussed in a separate paper, was of higher quality than the first two. If, again, we weight the cross sections inferred from individual capsules from the three runs, we find

$$\sigma_7(n,x\alpha) = 329 \text{ mb} \pm 16 \text{ mb} \quad (E_n = 15 \text{ MeV}),$$

where the uncertainty represents the spread in the measurements.

VI.C. ENDF/B-V.2. Cross Sections

The TART code utilizes a cross section library which has been developed at LLNL.[20] To facilitate comparison to the more popular ENDF set, the latest version[21] being ENDF/B-V.2, TART calculations were repeated with this set of cross sections for ^{6}Li, ^{7}Li, and deuterium. First a simple

representation of the ^{6}LiD cylindrical assembly was employed, and then we used a point source in a ^{6}LiD sphere, large enough to insure no leakage.

The results were quite similar. For an infinite medium of ^{6}LiD (95.5% ^{6}Li, 4.5% ^{7}Li), and E_n = 14.1 MeV, the ENDL set of Sept. 18, 1984 gave 1.26 tritons per neutron and 2.01 ^{4}He atoms per neutron. The ENDF/B-V.2 set gave 1.27 and 2.01, respectively. We see excellent agreement here. For the simple representation of the ^{6}LiD assembly, ratio of results using ENDF/B-V.2 to those using ENDL for both tritium and ^{4}He are plotted on Figs. 7 and 8. In the case of tritium production, we see that the ENDF/B-V.2 set leads to 1-2% more tritium than the ENDL set, an amount well within experimental uncertainty. For ^{4}He production, the two sets agree well except at shallow depths. A likely explanation is based on the difference in cross sections for the ^{6}Li(n,n'd)α reaction, with ENDF/B-V.2 values lower than those of the ENDL set. The role of this reaction becomes subordinate to the ^{6}Li(n,t)α reaction as greater depths are attained.

VII. Summary

We have measured, within a ^{6}LiD cylindrical assembly bombarded with D-T neutrons, the tritium produced in samples of ^{6}LiH and the ^{4}He produced in samples of ^{6}Li and ^{7}Li metal. Two separate and similar irradiations were performed. The tritium and ^{4}He measurements were carefully compared with TART Monte Carlo calculations. Special efforts were expended to keep overall uncertainties below 8%. The major contributor to the overall uncertainty was that associated with the neutron source strength determination, which relied primarily on four families of activation foils, all threshold detectors.

We found that TART predictions agreed well with the experiments. If we weight the measurements made along the ^{6}LiD axis according to (tritium/g ^{6}Li), we find:

$$\overline{(T_{exp.}/T_{calc.})}_{^{6}LiH} = 1.055 \pm 0.07 \quad .$$

Within experimental error, TART agrees with the experimental findings.

The ^{4}He experimental findings are also in good agreement with TART. For ^{4}He in ^{6}Li capsules, after weighting according to (^{4}He/g ^{6}Li), we find:

$$\overline{(^{4}He_{exp}/^{4}He_{calc})}_{^{6}Li} = 1.01 \pm 0.06 \quad .$$

The ^{7}Li results were of poorer quality, in large measure because of the relatively rapid dropoff of ^{4}He generated per capsule at greater depths into the ^{6}LiD.

TART calculations were also done with ENDF/B-V.2 cross sections. For the ^{6}LiD assembly geometry, we found that the ENDF/B-V.2 set leads to 1-2% more tritium than ENDL, while the ^{4}He generation is unchanged except at very shallow depths. Here, because the $^{6}Li(n,n'd)\alpha$ cross sections in ENDF/B-V.2 are smaller than those in the ENDL set, the ratio is 0.9 at the ^{6}LiD surface, and rises rapidly to unity at a depth of 70 mm. Therefore, the ENDF/B-V.2 set leads to 1% less ^{4}He than the ENDL set.

Acknowledgments

We are grateful to E. W. Burke for his sustained interest and support throughout the study. Many others contributed significantly, with good cheer, in the development and fabrication of detectors and major hardware. E. F. Plechaty and J. R. Kimlinger helped to make our use of TART a friendly experience. We thank also I. D. Proctor and the operating and maintenance staff for the virtually trouble-free performance of the RTNS-I facility through out the activity. D. W. Kneff and B. M. Oliver of Rockwell International Energy Systems Group were very responsive in their careful analyses of the ^{4}He-bearing capsules, easing our burdens through the development phase. We are indebted to V. C. Rupert and R. W. Bauer for translations of the abstract. This work was performed under the auspices of the U.S. Department of Energy by the Lawrence Livermore National Laboratory under contract number W-7405-ENG-48.

References

1. M. E. Wyman, "An Integral Experiment to Measure the Tritium Production from ^{7}Li by 14 MeV Neutrons in a Lithium Deuteride Sphere," LA-2234, Rev., Los Alamos Scientific Laboratory (1972).
2. R. Herzing, L. Kuyjpers, P. Cloth, D. Filges, R. Hecker, and N. Kirch, Nucl. Sci. Eng., 60, 169 (1976).
3. H. Bachmann, J. Fritscher, F. W. Kappler, D. Rusch, H. Werle, and H. W. Wiese, Nucl. Sci. Eng., 67, 74 (1978).
4. A. Hemmindinger, C. E. Ragan, and J. M. Wallace, Nucl. Sci. Eng., 70, 274 (1979).
5. H. Maekawa, K. Tsuda, T. Iguchi, Y. Ikeda, Y. Oyama, T. Fukumoto, Y. Seki, and T. Nakamura, "Measurements of Tritium Production-Rate Distribution in Simulated Blanket Assemblies at FNS," NEACRP-L-268, Department of Reactor Engineering, Tokai Research Establishment, JAERI (1983).
6. P. Cloth, D. Filges, H. Geiser, R. Herzing, G. L. Stocklin and R. Wolfle, Proc. 8th Symposium on Fusion Technology, Noorwijkerhowt, The Netherlands, 17-21 June 1974.
7. P. W. Benjamin, H. Goodfellow, J. Gray, J. W. Weale, Measurements of Neutron Reaction Rates Produced by a 14 MeV Neutron Source at the Centre of a Cylindrical Lithium Pile, AWRE Report No. NR 4/64, Aldermaston, Berks, 1964.
8. E. F. Plechaty and J. R. Kimlinger, "TARTNP Coupled Neutron-Photon Monte Carlo Transport Code," UCRL 50400, Vol. 14, Lawrence Livermore Laboratory (1975).

9. E. Goldberg, R. L. Barber, P. E. Barry, N. A. Bonner, J. E. Fontanilla, C. M. Griffith, R. C. Haight, D. R. Nethaway, and G. B. Hudson, Nucl. Sci. Eng., 91, 173 (1985).

10. R. Booth, J. C. Davis, C. L. Hanson, J. L. Held, C. M. Logan, J. E. Osher, R. A. Nickerson, B. A. Pohl and B. J. Schumacher, Nucl. Instrum. Methods 145, 25 (1977).

11. R. Booth and H. H. Barschall, Nucl. Instrum. Methods 99, 1 (1972).

12. D. W. Kneff, B. M. Oliver, H. Farrar IV, L. R. Greenwood, and F. M. Mann, submitted for publication in Nucl. Sci. Eng.

13. J. D. Seagrave, "D(D,n)^{3}He and T(D,n)^{4}He Neutron Source Handbook," LAMS-2162, Los Alamos National Laboratory (1958).

14. J. H. Ormrod, Nucl. Instrum. Methods 95, 49 (1971); see also H. H. Anderson and J. F. Ziegler, "Hydrogen Stopping Powers and Ranges in All Elements," Vol. 3 of The Stopping and Ranges of Ions in Matter, organized by J. F. Ziegler, New York: Pergammon (1977).

15. D. R. Nethaway, Private Communication (1983); see also D. R. Nethaway, Nucl. Phys. A190, 635 (1972), and J. Inorg. Nucl. Chem. 40, 1285 (1978).

16. S. Tagesen and H. Vonach, Physics Data 13-3, Karlsruhe (1981).

17. A. Pavlik, G. Winkler, H. Vonach, A. Paulsen and H. Liskien, J. Phys. G: Nucl. Phys. 8, 1283 (1982).

18. H. Farrar IV, W. N. McElroy, and E. P. Lippincott, Nucl. Technol. 25, 305 (1975).

19. G. J. Thomas, W. A. Swansiger, and M. I. Baskes, J. Appl. Phys. 50, 6942 (1979); see also C. L. Bisson and W. D. Wilson, Proceedings, Tritium Technology in Fission, Fusion and Isotopic Applications, Dayton, Ohio, Apr. 29-May 1, 1980, American Nuclear Society National Topical Meeting.

20. R. J. Howerton, R. E. Dye and S. T. Perkins, "Evaluated Nuclear Data Library," UCRL 50400, Vol. 4, Rev. 1, Lawrence Livermore National Laboratory (1981); cross section set used was TL831128.

21. ENDF/B-V2, ^{6}Li(Mat 1303, Mod 1), evaluated by G. Hale, L. Stewart and P. G. Young, Los Alamos National Laboratory (1977); also, ENDF/B-V2, ^{7}Li(Mat 1397, Mod 1), evaluated by P. G. Young, Los Alamos National Laboratory (1983); also, ENDF/B-V, D(Mat 1302), evaluated by L. Stewart, Los Alamos National Laboratory and A. Horsley, Aldermaston Laboratory (1978).

Table I

Parameters of the ^{6}LiD Assembly Components

Item	I.D. (mm)	O.D. (mm)	Thickness (mm)	Mass (kg)	Density (Mg/m^3)
Shroud	460.25	901.22	149.9	54.40	0.770
Block 1	26.67	901.57	248.9	122.90	0.774
Block 2	26.64	900.94	247.9	122.56	0.776

Table II. Contents of Sample Tube, First Irradiation

Station	Foils (Diameter, mm)	Capsule Cup	Wafer	Spacer (mm)	Measured Position[a] (mm)
1	Au, Nb (25.4)	-	-	-	0.00
2	Au, Nb, Ni (12.7)	-	-	-	6.46
3	Au, Nb, Ni (")	-	-	-	16.73
4	Au, Nb, Ni (")	-	-	-	27.06
5	Au, Nb, Ni, Zr (12.7)	-	-	-	37.44
6	Au, Zr, Y, Nb (25.4)	^{6}Li, ^{7}Li	^{6}LiH	-	48.86
7	Au, Zr, Y, Nb (")	^{6}Li, Pb	^{6}LiH	-	59.34
8	Au, Zr, Y, Nb (")	^{6}Li, ^{7}Li	^{6}LiH	^{6}LiD (10)	70.01
9	Au, Zr, Y, Nb (")	^{6}Li, Pb	^{6}LiH	^{6}LiD (")	90.59
10	Au, Zr, Y, Nb (")	^{6}Li, ^{7}Li	^{6}LiH	^{6}LiD (")	110.98
11	Au, Zr, Y, Nb (")	^{6}Li, Pb	^{6}LiH	^{6}LiD (")	131.50
12	Au, Zr, Y, Nb (")	^{6}Li, ^{6}Li	^{6}LiH	^{6}LiD (")	152.11
13	Au, Zr, Y, Nb (")	^{6}Li, ^{7}Li	^{6}LiH	^{6}LiD (20)	172.89
14	Au, Zr, Y, Nb (")	^{6}Li, ^{6}Li	^{6}LiH	^{6}LiD (")	203.53
15	Au, Zr, Y, Nb (")	^{6}Li, ^{6}Li	^{6}LiH	^{6}LiD (30)	233.96
16	Au, Zr, Y, Nb (")	^{6}Li, ^{6}Li	^{6}LiH	^{6}LiD (40)	274.59
17	Au, Zr, Y, Nb (")	^{6}Li, Pb	^{6}LiH	^{6}Li (220)	325.06

a. Relative to station 1.

Table III

Summary of Tritium Measurements in ^{6}LiH Wafers Exposed in First RTNS-I Irradiation

Station No.	$(\Delta Z)^a$ (mm)	T/liter H_2 x 10^{-12}	$(T-B)(\Delta Z)^2$ x 10^{-14}
6	59.8	8.21	2.92
7	70.4	7.70	3.79
8	81.0	7.27	4.73
9	101.5	6.17	6.30
10	122.1	5.63	8.32
11	142.7	4.25	8.55
12	163.2	- [d]	-
13	183.8	2.84	9.44
14	214.3	2.08	9.31
15	244.9	1.61	9.37
16	285.5	1.03	7.96
17	336.0	0.65	6.75

[a] Distance from source to center of wafer.
[b] Tritium atoms per liter H_2(STP).
[c] Tritium atoms $\cdot$ mm^2 $\cdot$ (liter H_2)$^{-1}$; B = background, 4.9 $\pm$ 1.5 x 10^{10} atoms tritium per liter H_2(STP).
[d] Rejected because of sample fractionation.

Table IV

^4He Measurements in ^6Li and ^7Li Capsules for Irradiation 1

at RTNS-I, S = 2.98×10^{17}n

Capsule No.			Li Mass (mg)		ΔZ^a (mm)	$^4He^b \times 10^{-10}$		$(\Delta Z)^2 \times (^4He - B)^c \times 10^{-12}$	
^6Li	^7Li	Pb	^6Li	^7Li		^6Li	^7Li	^6Li	^7Li
9	11		60.9	70.1	53.8	344	164	98.7	46.9
11		A	61.0		64.4	256		105	
10	12		62.0	70.5	74.9	216	93.7	118	51.2
12		B	60.3		95.5	150		137	
13	13		62.3	69.5	116.1	111	32.9	144	42.1
14		C	60.8		136.6	85.0		157	
6			60.1		157.2	66.0		163	
7			59.5		157.2	65.3		162	
5	14		59.4	69.7	177.7	51.4	11.6	162	31.1
4			59.7		208.3	51.2		222	
1			59.9		208.3	71.3		278	

[a] Distance from source to center of capsule
[b] Atoms of ^4He per capsule
[c] Backgrounds; ^6Li: 7.6×10^9; ^7Li: 1.8×10^{10}; Pb A, B: 4.7×10^9 each; Pb C was not measured.

Figure 1. Physical arrangement of the experiment. Details are shown for the components within the sample hole and also for the activation foil holder and contents protruding from the sample holder.

Figure 2. TART Monte Carlo geometric representation of ^{6}LiD assembly and rotating target assembly for the first irradiation.

Figure 3. Measured and calculated activities of zirconium, yttrium, niobium, and gold foils as a function of axial distance from the plane for first irradiation. For the calculated values, the source strength $S = 2.98 \times 10^{17}$ n was used. The function, $(Z)^2$ x (atoms of product/gm of sample) vs Z illustrates the attenuation due to the ^{6}LiD.

Figure 4. Measured and calculated tritium generated per liter of hydrogen as a function of axial distance for the first irradiation. The source strength is taken to be 2.99×10^{17} n. The line represents findings from an idealized TART calculation with fine statistics.

Figure 5. Measured and calculated ^{4}He generated per ^{6}Li capsule as a function of axial distance for first irradiation. Also included is a line inferred from a TART calculation with simpler geometry and better statistics. The source strength was taken to be 2.99×10^{17} n.

Figure 6. Measured and calculated activities of zirconium, yttrium, niobium, and gold foils as a function of axial distance from source plane for the second irradiation. $S = 4.99 \times 10^{17}$ n was used in the determination of the calculated points.

Figure 7. Ratio of experimentally determined tritium generated per wafer of ^{6}LiH to calculated values. Findings from Irradiations 1 and 2 are illustrated. Uncertainties represent total of contributions from experiment and calculation. See text for explanation of solid line.

Figure 8. Ratio of experimentally determined ^{4}He generated per capsule to calculated values. Findings from Irradiations 1 and 2 are shown. The cumulative uncertainties are illustrated.

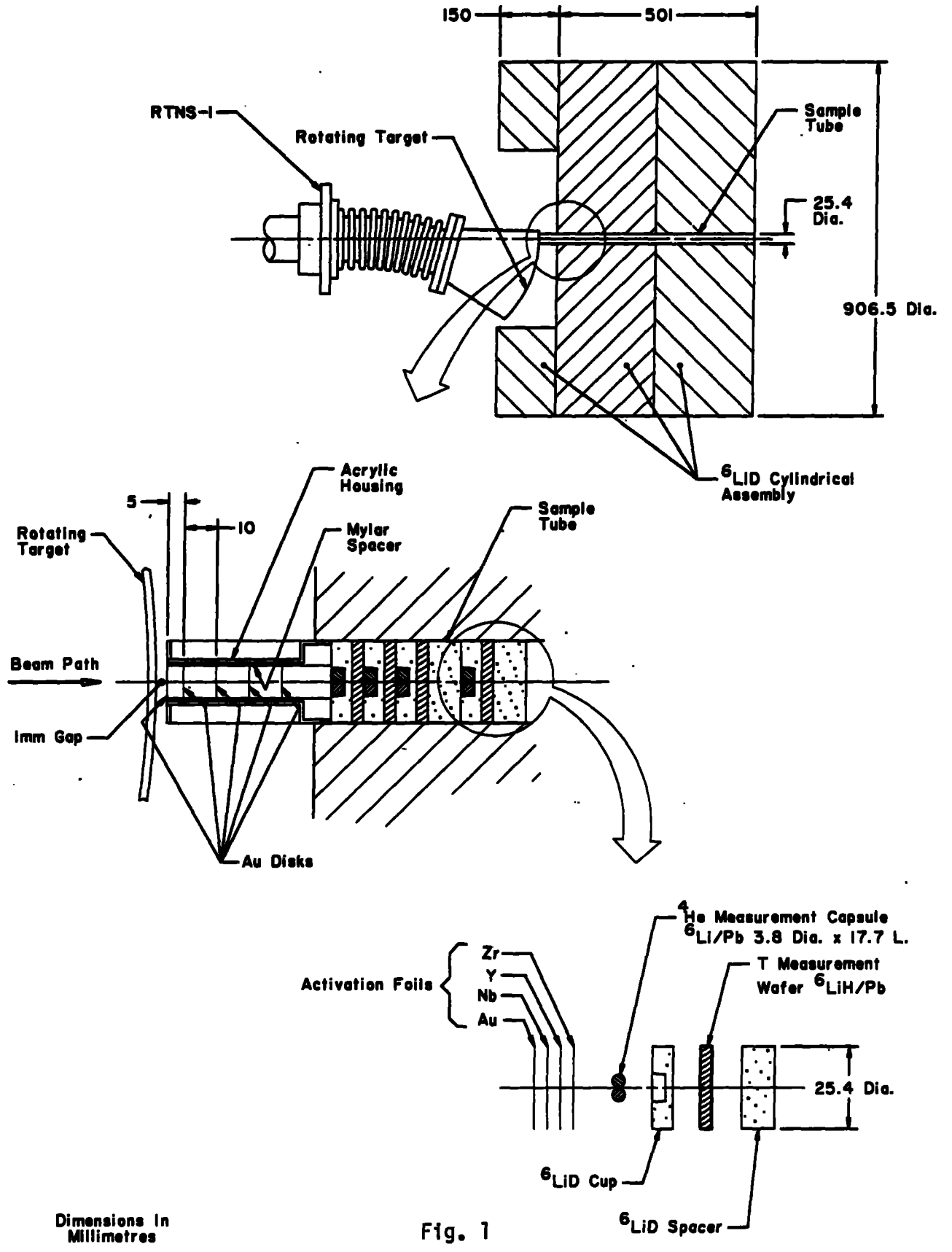

Dimensions In Millimetres

Fig. 1

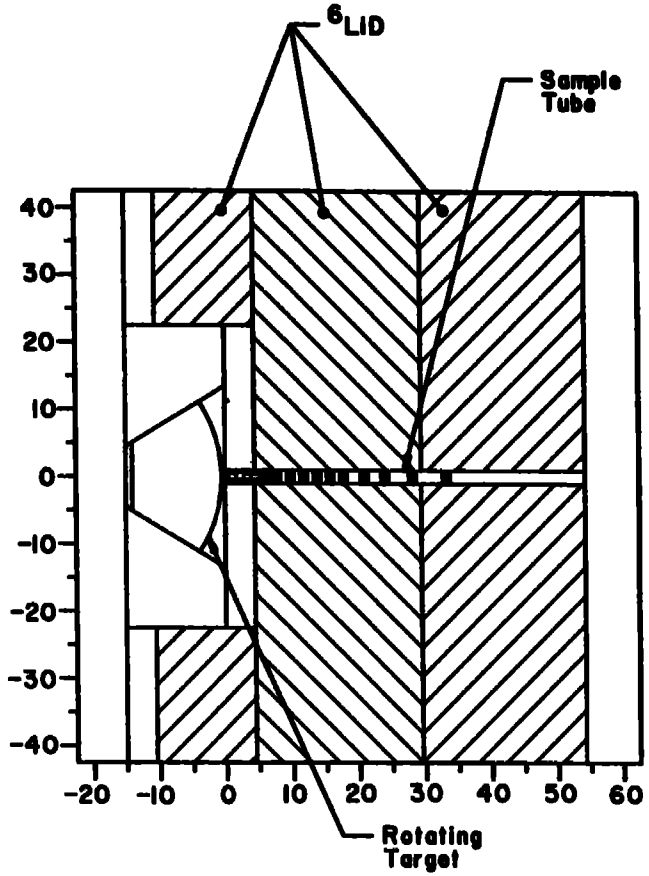
6 LID
Sample Tube
40
30
20
10
0
-10
-20
-30
-40
-20
-10
0
10
20
30
40
50
60
Rotating Target

Fig. 2

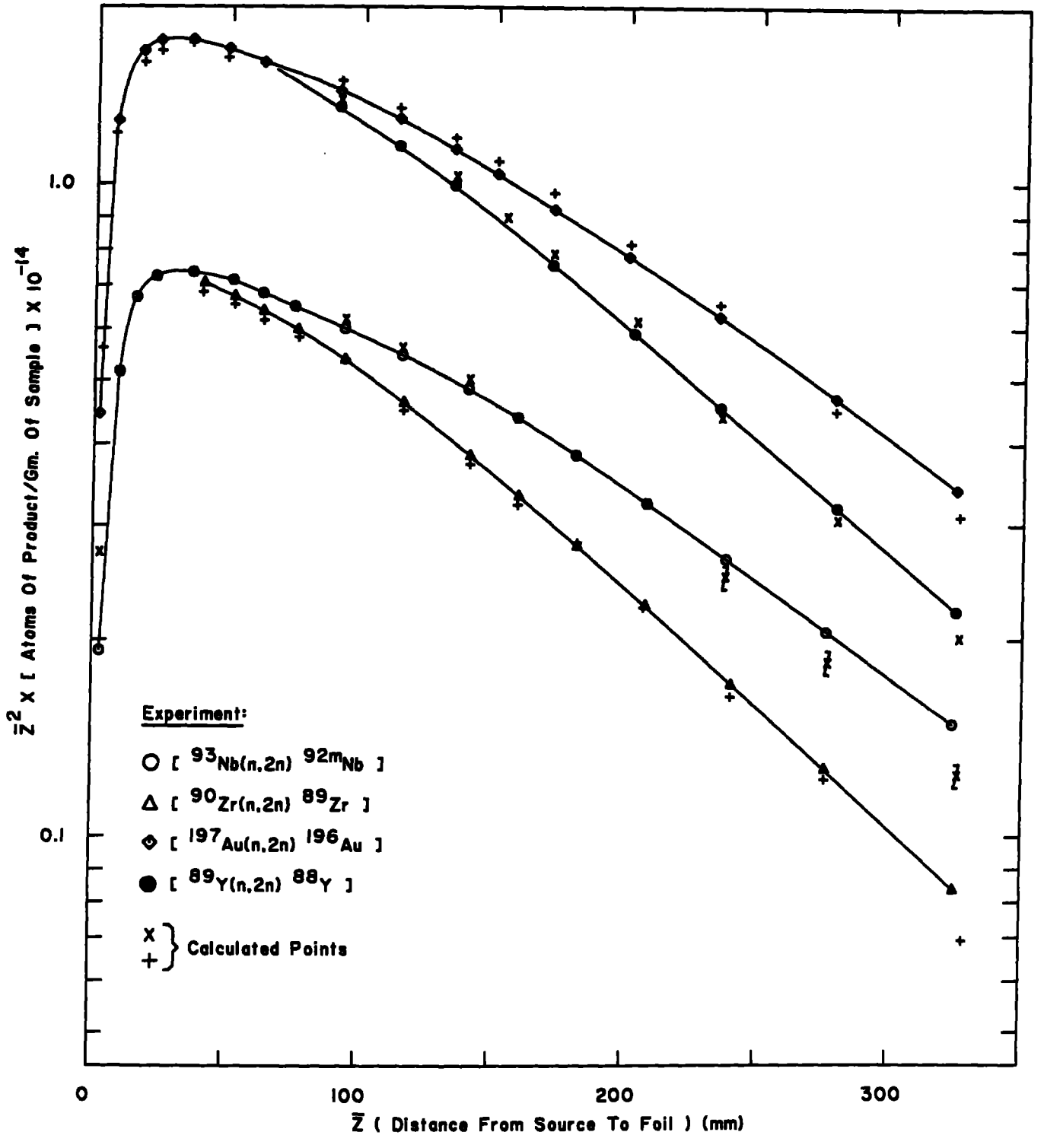
1.0
0.1
$\bar{Z}^2$ X [Atoms Of Product/Gm. Of Sample] X 10^{-14}
Experiment:
○ [$^{93}Nb(n,2n)\ ^{92m}Nb$]
△ [$^{90}Zr(n,2n)\ ^{89}Zr$]
◇ [$^{197}Au(n,2n)\ ^{196}Au$]
● [$^{89}Y(n,2n)\ ^{88}Y$]
X
+
Calculated Points
0
100
200
300
$\bar{Z}$ (Distance From Source To Foil) (mm)

Fig. 3

ooo Experiment
xxx TART
— TART, Idealized Geometry, Fine Statistics
1.0
0.1
0
200
400
600
$\bar{Z}^2$ x [Atoms Tritium/Liter H_2 (STP)] x 10^{-14}
$\bar{Z}$ (Source-Wafer Spacing) (mm)

Fig. 4

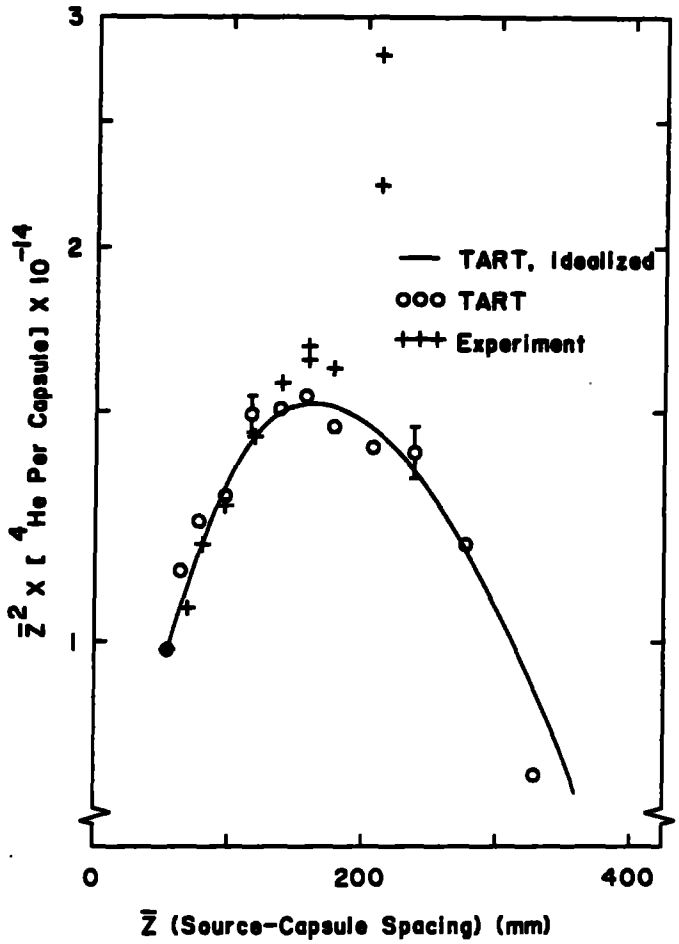
3
2
1
0
200
400
— TART, Idealized
ooo TART
+++ Experiment
$\bar{Z}^2 \times [\ ^4He\ Per\ Capsule] \times 10^{-14}$
$\bar{Z}$ (Source-Capsule Spacing) (mm)

Fig. 5

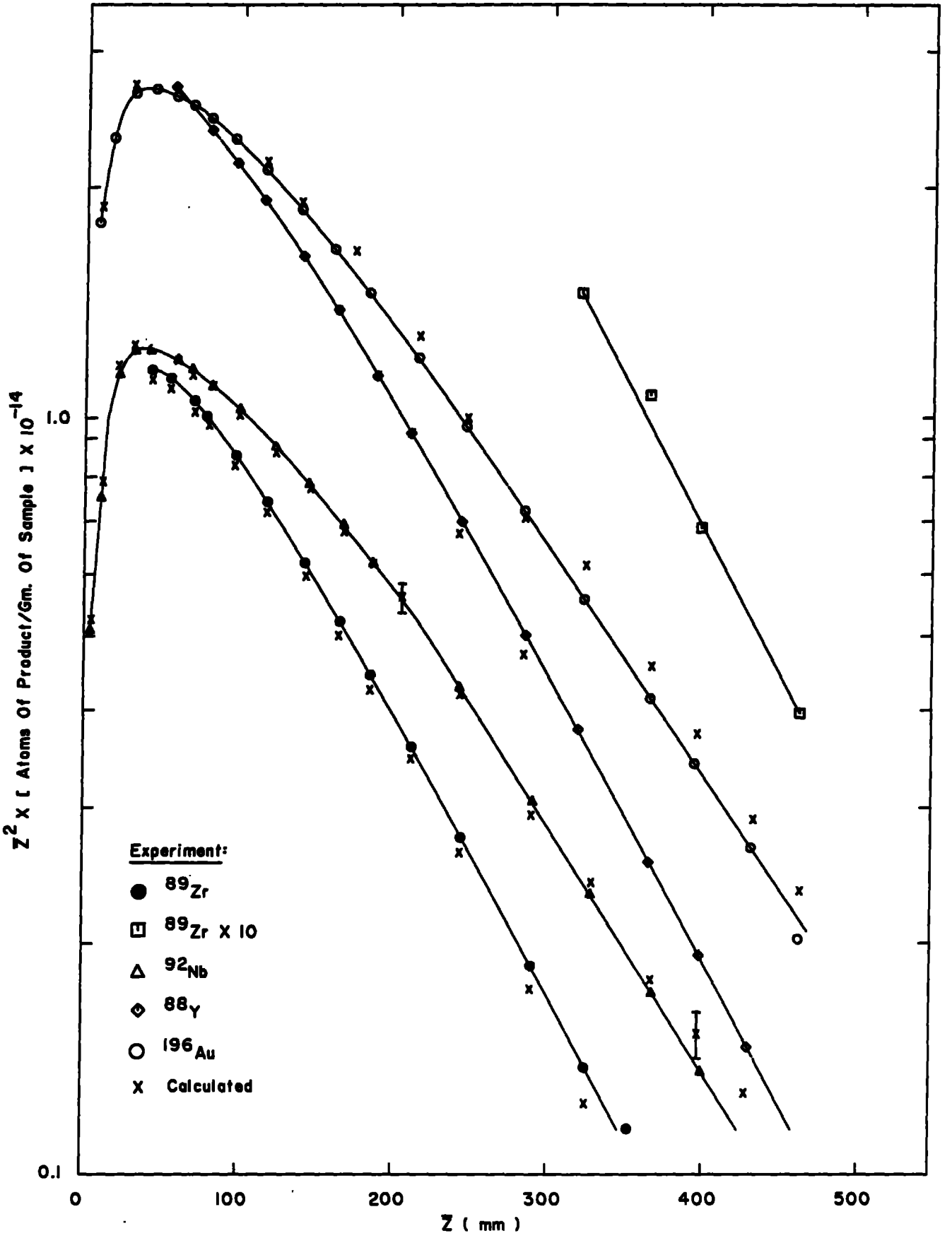
Z^2 X (Atoms Of Product/Gm. Of Sample) X 10^{-14}
1.0
0.1
0
100
200
300
400
500
Z (mm)
Experiment:
^{89}Zr
^{89}Zr X 10
^{92}Nb
^{88}Y
^{196}Au
Calculated

Fig. 6

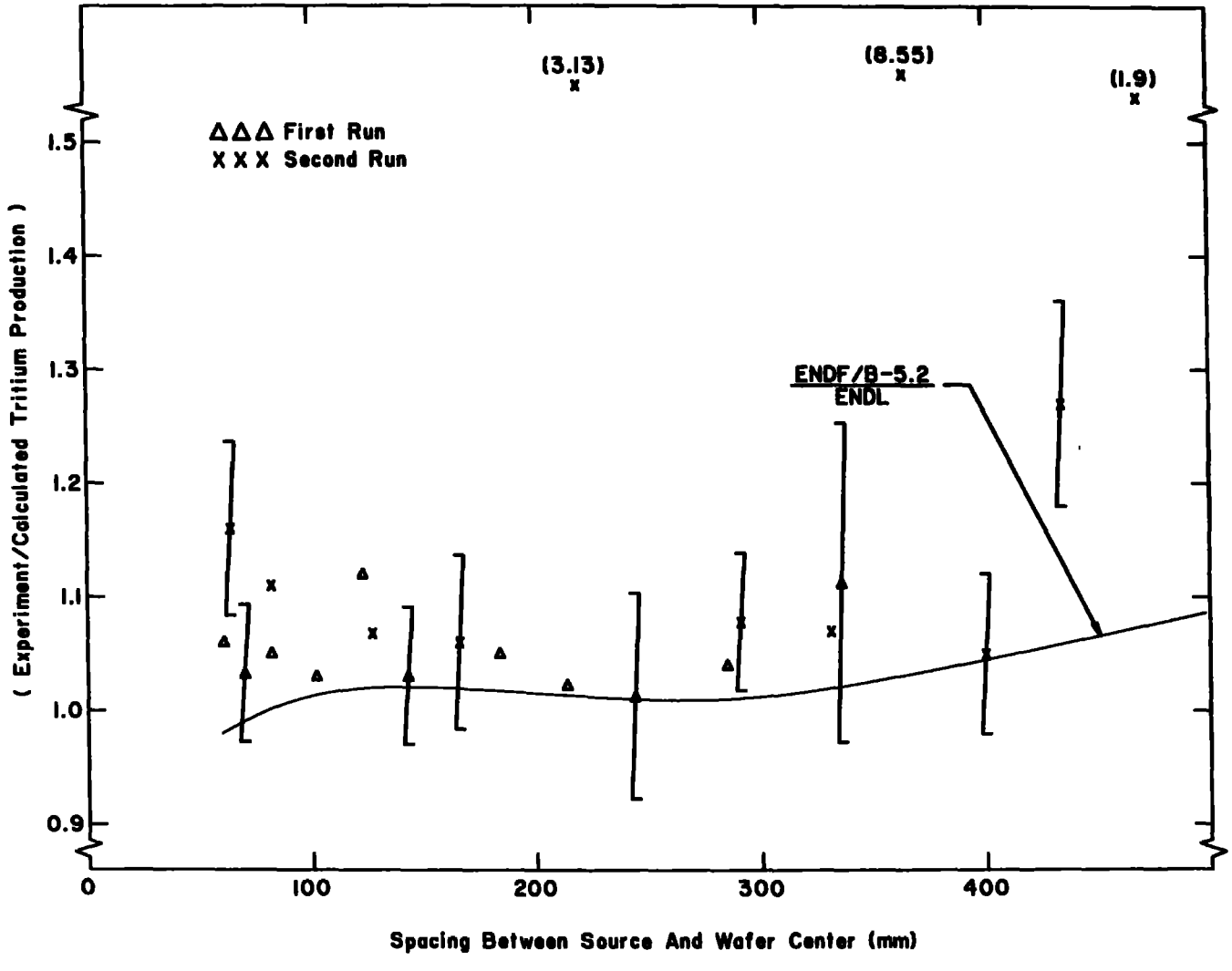
(3.13)
(8.55)
(1.9)
ΔΔΔ First Run
X X X Second Run
ENDF/B-5.2
ENDL
(Experiment/Calculated Tritium Production)
1.5
1.4
1.3
1.2
1.1
1.0
0.9
0
100
200
300
400
Spacing Between Source And Wafer Center (mm)

Fig. 7

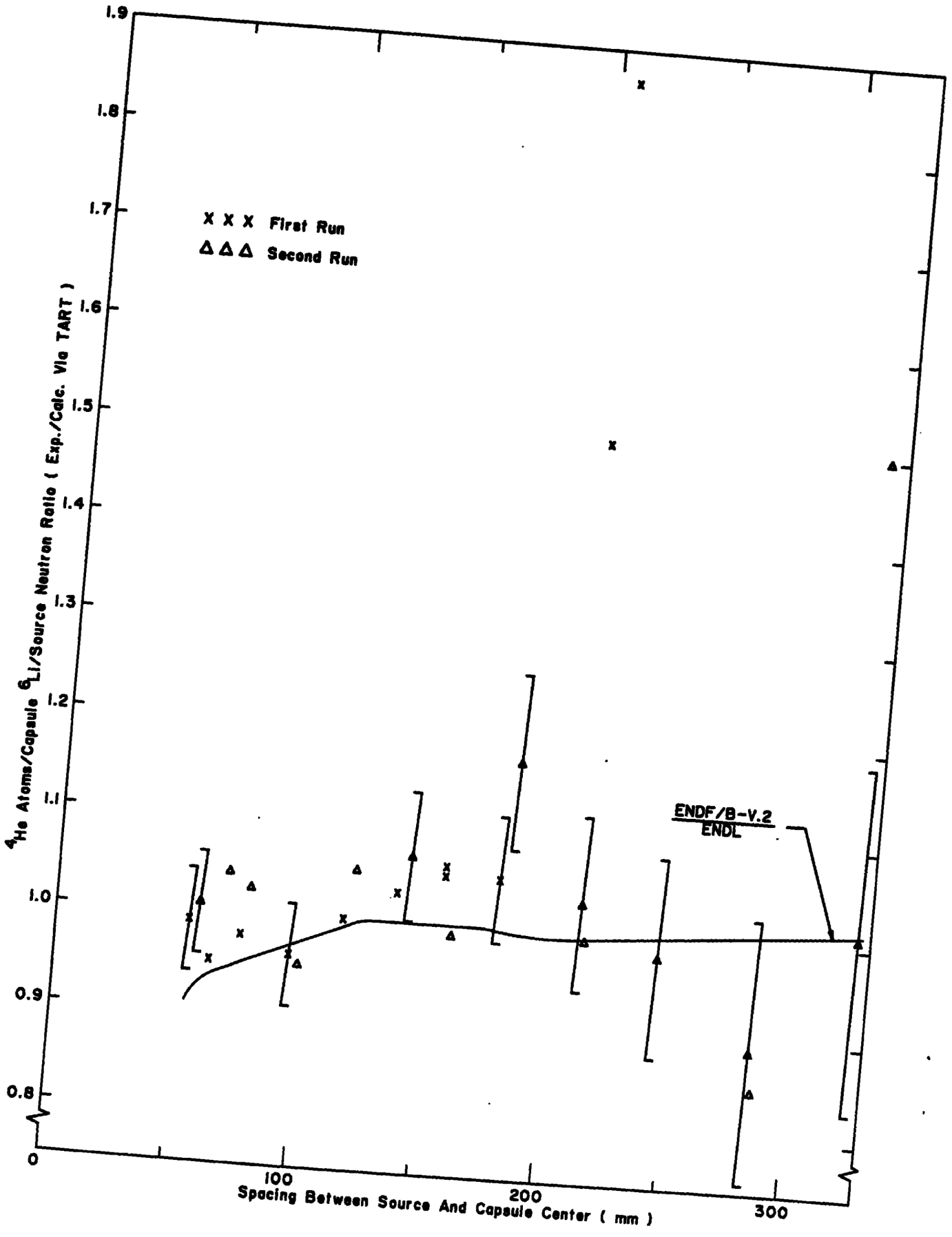
1.9
1.8
1.7
1.6
1.5
1.4
1.3
1.2
1.1
1.0
0.9
0.8
0
100
200
300
X X X First Run
Δ Δ Δ Second Run
ENDF/B-V.2
ENDL
^4He Atoms/Capsule ^6Li/Source Neutron Ratio (Exp./Calc. Via TART)
Spacing Between Source And Capsule Center (mm)

Fig. 8